Supplementary Information

First-Principles Investigation of $CuBiSeCl_2$: A Quaternary Halide Chalcogenide Material for Advanced Optoelectronic and Thermoelectric Energy Harvesting and Conversion Technologies

Zihad Hossain[1], Md. Riad Khan[1], Sanzida Naznin Mim[1], Md. Emon Hassan[1], Mohammad Abdur Rashid[2], Md. Lokman Ali[1]*
[1]Department of Physics, Pabna University of Science and Technology, Pabna-6600, Bangladesh
[2]Department Physics, Jashore University of Science and Technology Jashore 7408, Bangladesh
Corresponding Author's e-mail: lokman.cu12@gmail.com

Supplementary Methods:

Basis set convergence test

To ensure the reliability of our calculations, we carefully performed a basis set convergence test with respect to the RK_{max} parameter (R_{MT}×Rmax). The total energy was monitored as a function of RK_{max}, as illustrated in Fig.1.

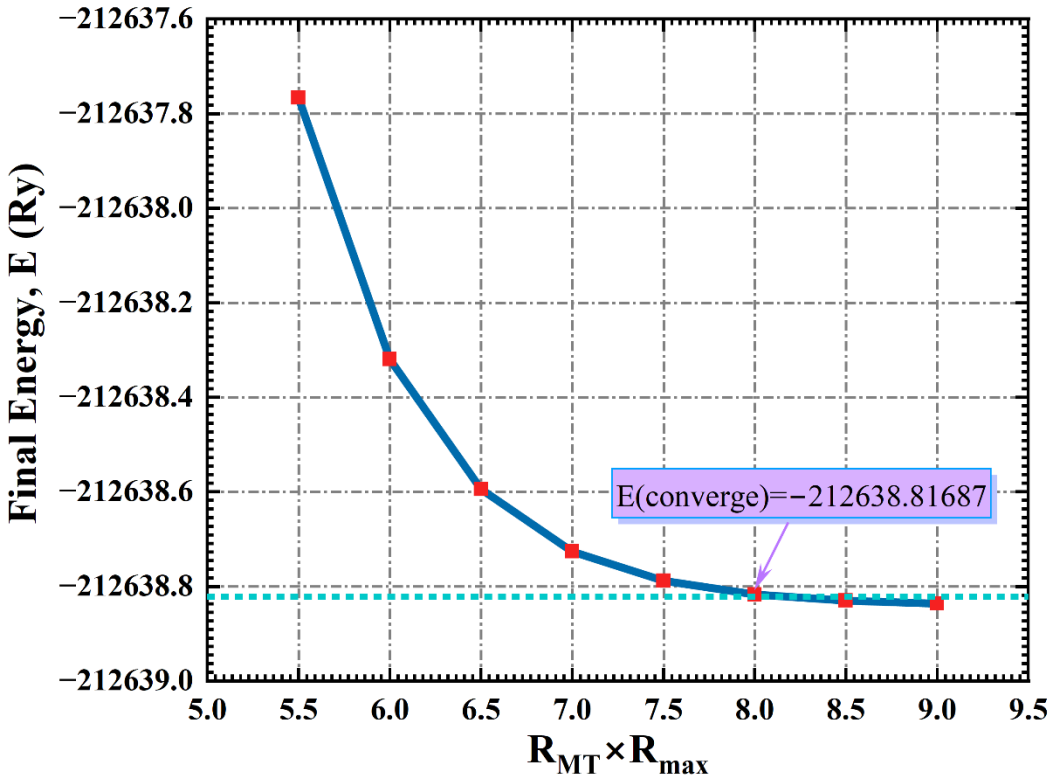

Fig. 1. Converge curve, the total energy is a function of RKmax.

The results show that the total energy decreases sharply at lower RK_{max} values and gradually approaches a constant value beyond RK_{max} = 8.0. The converged total energy was obtained as

E = –212638.81687 Ry, and further increase of RK_{max} from 8.0 to 9.0 resulted in a negligible energy variation of less than 1×10^{-4} Ry (≈ 1.36 meV/atom). This indicates that the total energy and derived quantities are fully converged with respect to RK_{max}. Therefore, RK_{max} = 8.0 was adopted for all subsequent calculations, as it ensures numerical stability and an optimal balance between accuracy and computational cost. The convergence criterion was set so that the change in total energy remained below 1×10^{-4} Ry, which is a standard and rigorous threshold for accurate first-principles simulations. Additionally, we verified that increasing RK_{max} beyond the converged value did not alter the band structure, density of states, or optical properties, confirming that our chosen cutoff provides a stable and reliable energy baseline for all physical analyses.

Table S1. Calculated converge data of RK_{max} and total energy.

Rkmax	**Total Energy**
5.0	-212636.7181
5.5	-212637.7664
6.0	-212638.3197
6.5	-212638.5945
7.0	-212638.7263
7.5	-212638.788
8.0	-212638.8169
8.5	-212638.8302
9.0	-212638.8363

Formation Enthalpy and Cohesive Energy

Table S2: Calculated formation enthalpy and cohesive energy

Total enthalpy of CuBiSeCl2	Isolated Energy in eV				Cohecive energy in eV/atom
	Cu	Bi	Se	Cl	
-53179.8414	-3307.3865	-43163.0142	-4860.4467	-921.6282	-15.613
Total enthalpy of CuBiSeCl2	Bulk Energy in eV				Formation Energy in eV/atom
	Cu	Bi	Se	Cl	
-53179.8414	-3309.6858	-43163.0717	-4860.2954	-922.8887	-2.7514

2.1. Optical Constants: Calculation Methods

The frequency-dependent complex dielectric function is given by:

$$\varepsilon(\omega) = \varepsilon_1(\omega) + i\varepsilon_2(\omega) \tag{1}$$

where $\varepsilon_1(\omega)$ represents the real part, and $\varepsilon_2(\omega)$ accounts imaginary part. In cartesian coordinates,

$$\varepsilon(\omega) = \begin{pmatrix} \varepsilon_{xx}(\omega) & \varepsilon_{xy}(\omega) & \varepsilon_{xz}(\omega) \\ \varepsilon_{yx}(\omega) & \varepsilon_{yy}(\omega) & \varepsilon_{yz}(\omega) \\ \varepsilon_{zx}(\omega) & \varepsilon_{zy}(\omega) & \varepsilon_{zz}(\omega) \end{pmatrix} \tag{2}$$

At long-wavelength infrared (LWIR) wavelengths for the intra-band transitions the overall dielectric function can be represented by,

$$\varepsilon(\omega) = \varepsilon^{inter}(\omega) + \varepsilon^{intra}(\omega) \tag{3}$$

The derivation of the inter-band component of the dielectric function from first-order time-dependent perturbation theory [1],

$$\varepsilon^{inter}_{\alpha\beta}(\omega) = 1 - \frac{8\pi e^2}{\Omega} \sum_{k,v,c} \frac{\left\langle \psi_{k+qe_\alpha}^{c} \middle| e^{iq.r} \middle| \psi_k^v \right\rangle \left\langle \psi_k^v \middle| e^{-iq.r} \middle| \psi_{k+qe_\beta}^{c} \right\rangle}{(E_{k+q}^{c} - E_k^v - \hbar\omega - i\hbar\alpha)} + CC \tag{4}$$

In this formulation, Ω represents the volume of a single unit cell , the parameter q captures the photon momentum, ω symbolizes the phonon frequency, r defines the position vector, the elementary charge of an electron is represented by e,. Furthermore, E_k^v and E_{k+q}^{c} correspond to the wavefunctions of electrons in the valence and conduction bands at a specific wavevector k. Using the Kramers-Kronig relation,

$$\varepsilon_1^{inter}(\omega) = 1 + \frac{2}{\pi} P \int_0^\infty \frac{\omega' \varepsilon_2^{inter}(\omega') d\omega'}{\omega'^2 - \omega^2}. \tag{5}$$

With the help of the free-electron plasma model, the intra-band contributions to the dielectric function,

$$\varepsilon^{inter}(\omega) = 1 - \frac{\omega_p^2}{\omega(\omega + i\gamma)'} \tag{6}$$

Herein, The inverse lifetime (γ) may vary from 0 to 1 eV [2] and the complex optical conductivity (ω) is established based on the following relation:

$$\sigma(\omega) = -i\frac{\omega}{4\pi}[\varepsilon(\omega) - 1] \quad (7)$$

However, the optical properties can be determined with the help of the following equations [3]:

$$K(\omega) = \frac{I(\omega)}{2\omega} \quad (8)$$

$$I(\omega) = \sqrt{2}\omega\left(\sqrt{\varepsilon_1(\omega)^2 + \varepsilon_2(\omega)^2} - \varepsilon_1(\omega)\right)^{1/2} \quad (9)$$

$$L(\omega) = \frac{E}{(\varepsilon_1(\omega)^2 + \varepsilon_2(\omega)^2)} \quad (10)$$

$$r(\omega) = \frac{n + iK - 1}{n + iK + 1} \quad (11)$$

$$n(\omega) = \left(\frac{1}{\sqrt{2}}\right)\left(\sqrt{\varepsilon_1(\omega)^2 + \varepsilon_2(\omega)^2} - \varepsilon_1(\omega)\right)^{1/2} \quad (12)$$

$$\varepsilon_1(\omega) = n^2 - K^2 \quad (13)$$

$$\varepsilon_2(\omega) = 2nK \quad (14)$$

$$\sqrt{\varepsilon(\omega)} = n(\omega) + iK_{(\omega)} \quad (15)$$

2.2. Methods of elastic and mechanical properties

The mechanical performance of solids is fundamentally governed by the elastic stiffness constants C_{ij}, which describe the linear relationship between stress and strain within the elastic regime. These constants offer crucial insights into a material's structural stability, dynamic response, and hardness. To determine the elastic constants, stress - strain methods are employed, where small deformations are applied to the crystal structure to observe its mechanical response [4]. The expression below is used to compute the stress that counteracts the applied strain and restores equilibrium:

$$\begin{Bmatrix}\begin{pmatrix}\sigma_1\\ \sigma_2\\ \sigma_3\\ \tau_1\\ \tau_2\\ \tau_3\end{pmatrix} = \begin{pmatrix}C_{11} & C_{12} & C_{13} & C_{14} & C_{15} & C_{16}\\ C_{21} & C_{22} & C_{23} & C_{24} & C_{25} & C_{26}\\ C_{31} & C_{32} & C_{33} & C_{34} & C_{35} & C_{36}\\ C_{41} & C_{42} & C_{43} & C_{44} & C_{45} & C_{46}\\ C_{51} & C_{52} & C_{53} & C_{54} & C_{55} & C_{56}\\ C_{61} & C_{62} & C_{63} & C_{64} & C_{65} & C_{66}\end{pmatrix}\begin{pmatrix}\varepsilon_1\\ \varepsilon_2\\ \varepsilon_3\\ \gamma_1\\ \gamma_2\\ \gamma_3\end{pmatrix}\end{Bmatrix} \quad (16)$$

The symbols $\sigma_i, \tau_i, \varepsilon_i,$ and γ_i represents normal stress, Eulerian strain, and shear stress, respectively. This equation demonstrates how Hooke's law relates the stresses (σ_i, τ_i) to their corresponding strains (ε_i, γ_i) in a material.

Due to the lattice symmetry of the crystal structure, there are nine independent elastic constants: C_{11},C_{12},C_{13},C_{22},C_{23}, C_{33},C_{44},C_{55},, and C_{66}. For orthorhombic crystals at zero pressure, the mechanical stability must satisfy the Born stability criteria, which are expressed as follows: [5,6]:

$$\left\{\begin{array}{c} C_{11}>0; C_{22}>0; C_{33}>0; \\ C_{44}>0;\ C_{55}>0; C_{66}>0; \\ \left[C_{11}+C_{22}+C_{33}+2\left(C_{12}+C_{13}+C_{23}\right)\right]>0; \\ \left(C_{11}+C_{33}-2C_{12}\right)>0; \\ \left(C_{11}+C_{33}-2C_{13}\right)>0; \\ \left(C_{11}+C_{33}-2C_{23}\right)>0 \end{array}\right\} \tag{17}$$

The shear moduli (G) and bulk moduli (B) can be calculated using the Voigt-Reuss-Hill (VRH) approximation method [5,7,8]:

$$\left\{\begin{array}{l} B_H=\frac{1}{2}\left(B_R+B_v\right) \\ G_H=\frac{1}{2}\left(G_R+G_v\right) \end{array}\right\} \tag{18}$$

Here, B_v and B_R are the upper and lower bounds of the bulk modulus, calculated using the Voigt and Reuss methods. The Voigt Reuss bounds for B and G in the orthorhombic configuration are presented as follows:

$$\left\{\begin{array}{c} B_v=\frac{\left(C_{11}+C_{22}+C_{33}\right)+2\left(C_{12}+C_{13}\right)}{9} \\ B_R=\frac{\Delta}{\left[C_{11}*\left(C_{22}+C_{33}-2*C_{23}\right)+C_{22}*\left(C_{33}-2*C_{13}\right)-\right.} \\ \left(2*C_{33}*C_{12}\right)+C_{12}*\left(2*C_{23}-C_{12}\right)+C_{13}*\left(2*C_{12}-C_{13}\right) \\ \left.+C_{23}*\left(2*C_{13}-C_{23}\right)\right] \\ G_v=\frac{C_{11}+C_{22}+C_{33}+3*\left(C_{44}+C_{55}+C_{66}\right)-\left(C_{12}+C_{13}+C_{23}\right)}{15} \\ G_R=\frac{\begin{array}{c}[4\{C_{11}*\left(C_{22}+C_{33}+C_{23}\right)+C_{22}* \\ \left(C_{33}+C_{13}\right)+C_{33}*C_{12}-C_{12}*\left(C_{23}+C_{12}\right)-C_{13}* \\ \left(C_{12}+C_{13}\right)-C_{23}*\left(C_{13}+C_{23}\right)\}/\Delta\ +3\{(1/C_{44})+(1/C_{55})+(1/C_{66})\}]\end{array}}{15} \end{array}\right\} \tag{19}$$

Young's modulus (Y) and Poisson's ratio (ν) were determined, using the following formulas,

$$\left\{\begin{array}{c} Y = \dfrac{9B_H G_H}{3B_H + G_H} \\ \nu = \dfrac{3B_H - 2G_H}{2(3B_H + G_H)} \end{array}\right\} \tag{20}$$

To gain deeper insights into the mechanical behavior of $CuBiSeCl_2$, additional parameters such as the Kleinman parameter (ζ), machinability index (μ_m) were evaluated, as summarized in Table 4. The following formula were utilized to obtain them,

$$\left\{\begin{array}{c} \zeta = \dfrac{C_{11} + 8C_{12}}{7C_{11} + 2C_{12}} \\ \mu_M = \dfrac{B}{C_{44}} \\ \lambda = \dfrac{\nu E}{(1+\nu)(1-2\nu)} \end{array}\right\} \tag{21}$$

Hardness is a key mechanical property that reflects a material's resistance to deformation or indentation. In this study, the hardness of $CuBiSeCl_2$ was estimated using the theoretical model proposed by Chen et al. [9], along with additional semi-empirical formulas for hardness prediction [10] . The relevant equations are as follows:

$$\left\{\begin{array}{c} H_1 = 0.0963B \\ H_2 = 0.0607E \\ H_3 = 0.1475G \\ H_4 = 0.0635E \\ H_5 = -2.899 + 0.1769G \\ H_6 = \dfrac{(1-2\nu)B}{6(1+\nu)} \\ H_7 = \dfrac{(1-2\nu)E}{6(1+\nu)} \\ H_8 = 2(k^2G)^{0.585} - 3 = H_v \end{array}\right\} \tag{22}$$

Where *B* and *G* are Bulk and Shear modulus in GPa and $k = \dfrac{G}{B} = \dfrac{1}{Pugh's\ ratio}$.

The direction dependent characteristics of solids can be explained by anisotropy. To estimate elastic anisotropy, the universal index (A^U) is utilized [11].

$$\left\{A^U = 5\frac{G_V}{G_R} + \frac{B_V}{G_R} - 6\right\} \tag{23}$$

Some additional indicators of anisotropy are, shear anisotropy (A^G),[12], Zener anisotropy factor (A^Z), bulk anisotropy (A^B), equivalent Zener anisotropy factor (A^{eq})[13], log-Euclidean index (A^L) [12] are obtained by the below relations [14],

$$\left\{A^G = \frac{G_v - G_R}{2G_H}\right\} \tag{24}$$

$$\left\{A_1 = \frac{4C_{44}}{C_{11} + C_{33} - 2C_{13}}\right\} \tag{25}$$

$$\left\{A_2 = \frac{4C_{55}}{C_{22} + C_{33} - 2C_{23}}\right\} \tag{26}$$

$$\left\{A_3 = \frac{4C_{66}}{C_{11} + C_{22} - 2C_{12}}\right\} \tag{27}$$

$$\left\{A^B = \frac{B_V - B_R}{B_V + B_R}\right\} \tag{28}$$

$$\left\{A^Z = \frac{2C_{44}}{(C_{11} - C_{12})}\right\} \tag{29}$$

$$\left\{A^{eq} = \left(1 + \frac{5}{12}A^U\right) + \sqrt{\left(1 + \frac{5}{12}A^U\right)^2 - 1}\right\} \tag{30}$$

$$\left\{A^L = \sqrt{[\ln\left(\frac{B_V}{B_R}\right) + 5[\ln\left(\frac{C_{44}^V}{C_{44}^R}\right)]^2}\right\} \tag{31}$$

Here, C_{44}^v is the C_{44} values for Voigt and C_{44}^R is the same for Reuss, which can be expressed as-

$$\left\{\begin{matrix} C_{44}^R = \frac{5}{3} \frac{C_{44}(C_{11} - C_{12})}{3(C_{11} - C_{12}) + 4C_{44}} \\ C_{44}^V = \frac{3}{5} \frac{(C_{11} - C_{12} - 2C_{44})^2}{3(C_{11} - C_{12}) + 4C_{44}} \end{matrix}\right\} \tag{32}$$

Supplementary Results:

3. Results and Discussion

3.1. Structural Analysis with Ground-State Properties

Table S3: Energy configuration with volume.

Volume (Bohr³)	Volume (Å³)	ΔVol (%)	Total Energy (Ry)
2958.426	438.4444	-5	-212638.71641
2989.567	443.1787	-4	-212638.72147
3020.709	447.913	-3	-212638.72531
3051.85	452.6473	-2	-212638.72739
3082.992	457.3817	-1	-212638.72847
3114.133	462.116	0	-212638.72742
3145.274	466.8503	1	-212638.72552
3176.416	471.5847	2	-212638.72238
3207.557	476.319	3	-212638.71812
3238.698	481.0533	4	-212638.71275
3269.839	485.7876	5	-212638.70622

Table S4: Lattice parameters

Parameters		PBEsol	Exp.	Relative errors
Lattice Constants	a	8.75477	8.78415	0.38%
	b	3.98466	3.998	0.34%
	c	13.09603	13.13998	0.36%

3.2. Electronic Properties

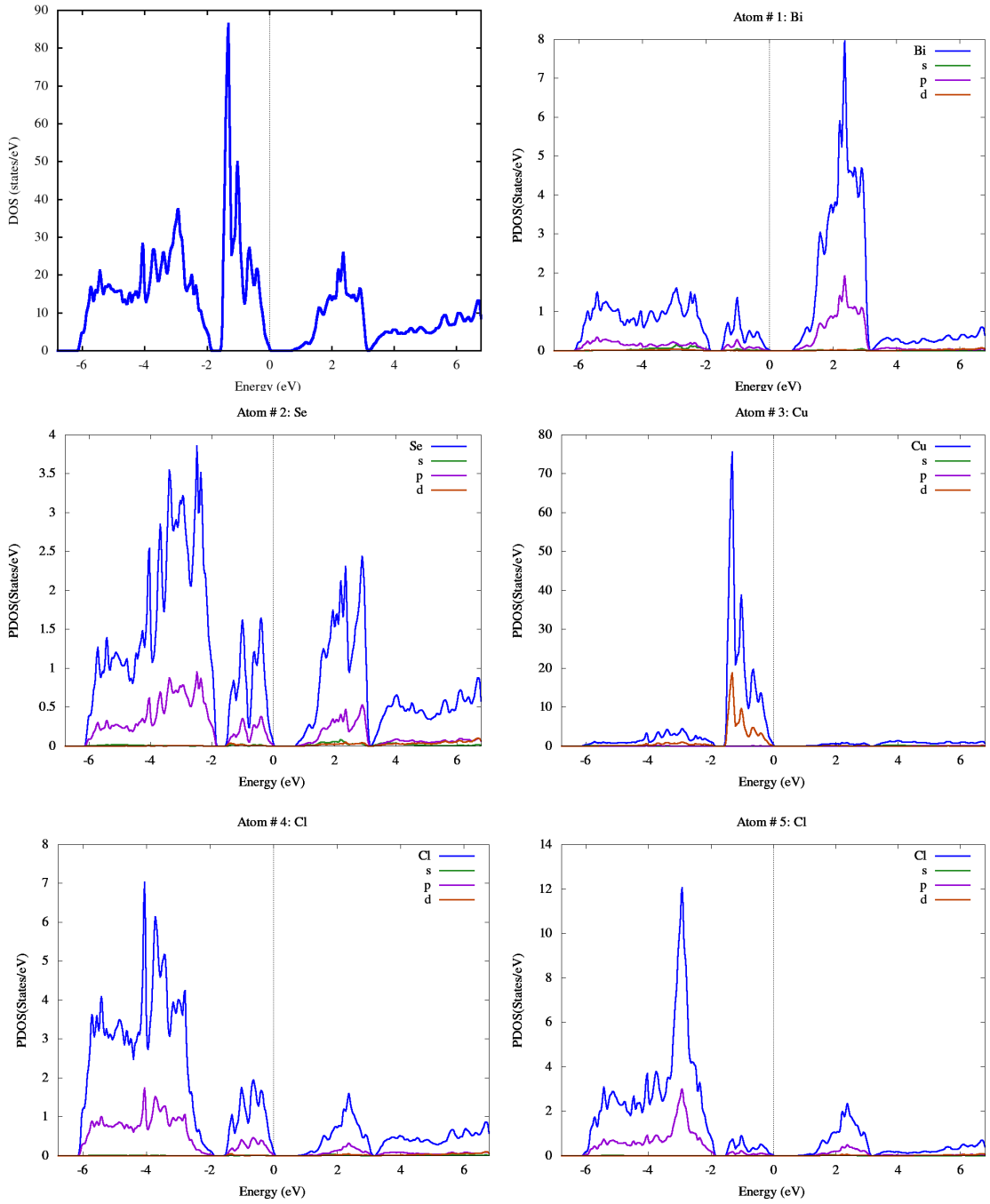

Fig. S2: Element- and orbital-resolved (s, p, d) PDOS analysis of $CuBiSeCl_2$.

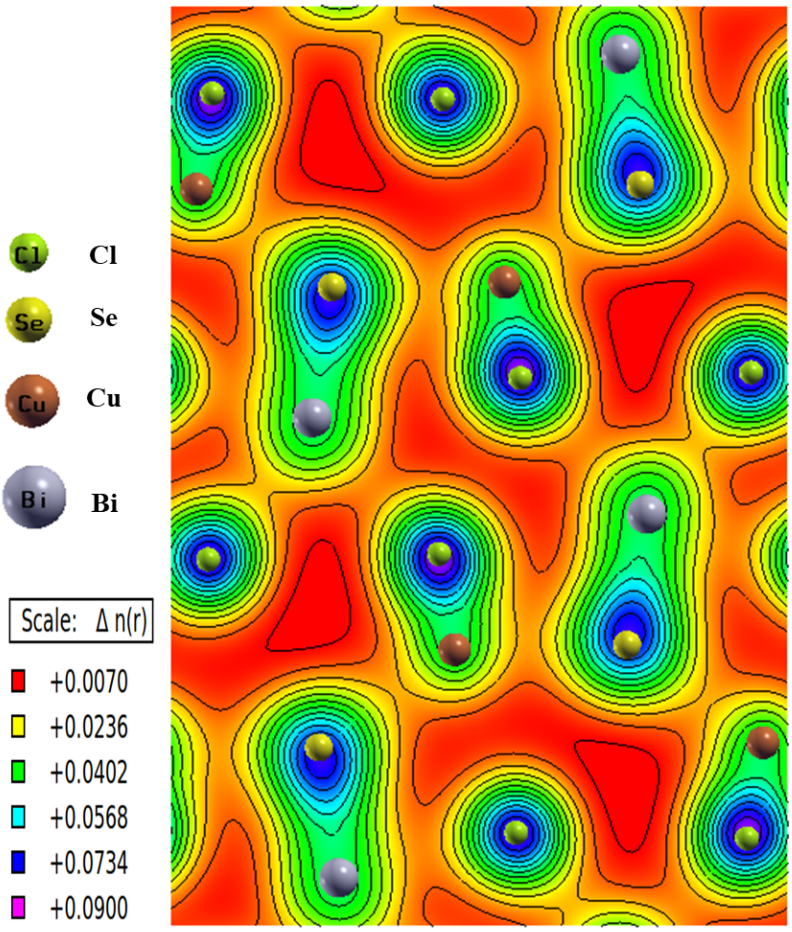

Fig. S3: Charge density analysis for Cu, Bi, Se, and Cl in $CuBiSeCl_2$.

References:

[1] S. Bharadwaj, T. Van Mechelen, Z. Jacob, Picophotonics: Anomalous Atomistic Waves in Silicon, Phys. Rev. Applied 18 (2022) 044065. https://doi.org/10.1103/PhysRevApplied.18.044065.

[2] M.J. Van Setten, S. Er, G. Brocks, R.A. De Groot, G.A. De Wijs, First-principles study of the optical properties of Mg x Ti 1 − x H 2, Phys. Rev. B 79 (2009) 125117. https://doi.org/10.1103/PhysRevB.79.125117.

[3] Md.L. Ali, Z. Hossain, S.N. Mim, S.K. Saha, Pressure Effects on Physical Properties of Binary Rare Earth Mono-Pnictide YBi for Optoelectronics Applications, Advanced Theory and Simulations n/a (n.d.) 2401066. https://doi.org/10.1002/adts.202401066.

[4] A. Dal Corso, Elastic constants of beryllium: a first-principles investigation, Journal of Physics: Condensed Matter 28 (2016) 075401.

[5] Z. Wu, E. Zhao, H. Xiang, X. Hao, X. Liu, J. Meng, Crystal structures and elastic properties of superhard Ir N 2 and Ir N 3 from first principles, Phys. Rev. B 76 (2007) 054115. https://doi.org/10.1103/PhysRevB.76.054115.

[6] H. Ozisik, K. Colakoglu, H.B. Ozisik, E. Deligoz, Structural, elastic, and lattice dynamical properties of Germanium diiodide (GeI2), Computational Materials Science 50 (2010) 349–355. https://doi.org/10.1016/j.commatsci.2010.08.026.

[7] R. Hill, The Elastic Behaviour of a Crystalline Aggregate, Proc. Phys. Soc. A 65 (1952) 349. https://doi.org/10.1088/0370-1298/65/5/307.

[8] D.G. Pettifor, Theoretical predictions of structure and related properties of intermetallics, Materials Science and Technology 8 (1992) 345–349. https://doi.org/10.1179/mst.1992.8.4.345.

[9] X.-Q. Chen, H. Niu, D. Li, Y. Li, Modeling hardness of polycrystalline materials and bulk metallic glasses, Intermetallics 19 (2011) 1275–1281.

[10] M.I. Naher, S.H. Naqib, Possible applications of Mo2C in the orthorhombic and hexagonal phases explored via ab-initio investigations of elastic, bonding, optoelectronic and thermophysical properties, Results in Physics 37 (2022) 105505.

[11] D. Engin, C. Kemal, C.Y. Oztekin, Ab initio study on hypothetical silver nitride, Chinese Physics Letters 25 (2008) 2154.

[12] C.M. Kube, Elastic anisotropy of crystals, AIP Advances 6 (2016). https://pubs.aip.org/aip/adv/article/6/9/095209/873497 (accessed August 17, 2024).

[13] S.I. Ranganathan, M. Ostoja-Starzewski, Universal Elastic Anisotropy Index, Phys. Rev. Lett. 101 (2008) 055504. https://doi.org/10.1103/PhysRevLett.101.055504.

[14] R. Gaillac, P. Pullumbi, F.-X. Coudert, ELATE: an open-source online application for analysis and visualization of elastic tensors, Journal of Physics: Condensed Matter 28 (2016) 275201.